catalysts

MDPI

Article

Novel Ni-Ce-Zr/Al_2O_3 Cellular Structure for the Oxidative Dehydrogenation of Ethane

Juan Pablo Bortolozzi [1,*], Raquel Portela [2], Pedro Ávila [2], Viviana Milt [1] and Eduardo Miró [1]

[1] Instituto de Investigaciones en Catálisis y Petroquímica—INCAPE (UNL-CONICET), Santiago del Estero 2829, S3000AOM Santa Fe, Argentina; vmilt@fiq.unl.edu.ar (V.M.); emiro@fiq.unl.edu.ar (E.M.)

[2] Instituto de Catálisis y Petroleoquímica, ICP (CSIC). Marie Curie 2, Cantoblanco, 28049 Madrid, España; raquel.portela@csic.es (R.P.); pavila@icp.csic.es (P.Á.)

* Correspondence: jpbortolozzi@fiq.unl.edu.ar; Tel.: +54-342-453-6861

Received: 4 October 2017; Accepted: 31 October 2017; Published: 8 November 2017

Abstract: A novel γ-alumina-supported Ni-Ce-Zr catalyst with cellular structure was developed for oxidative dehydrogenation of ethane (ODHE). First, powdered samples were synthesized to study the effect of both the total metal content and the Ce/Zr ratio on the physicochemical properties and performance of these catalysts. All synthesized powdered samples were highly active and selective for ODHE with a maximum ethylene productivity of 6.94 $\mu mol_{ethylene}\ g_{act\ cat}^{-1}\ s^{-1}$. According to the results, cerium addition increased the most reducible nickel species population, which would benefit ethane conversion, whereas zirconium incorporation would enhance ethylene selectivity through the generation of higher amounts of the least reducible nickel species. Therefore, the modification of active site properties by addition of both promoters synergistically increases the productivity of the Ni-based catalysts. The most efficient formulation, in terms of ethylene productivity per active phase amount, contained 15 wt% of the mixed oxide with $Ni_{0.85}Ce_{0.075}Zr_{0.075}$ composition. This formulation was selected to synthesize a Ni-Ce-Zr/Al_2O_3 structured body by deposition of the active phase onto a homemade γ-alumina monolith. The structured support was manufactured by extrusion of boehmite-containing dough. The main properties of the $Ni_{0.85}Ce_{0.075}Zr_{0.075}$ powder were successfully preserved after the shaping procedure. In addition, the catalytic performance of the monolithic sample was comparable in terms of ethylene productivity to that of the powdered counterpart.

Keywords: Ni-Ce-Zr; alumina cellular structure; oxidative dehydrogenation; Ethylene

1. Introduction

In recent years, the global demand for light olefins has steadily increased and this trend is expected to continue in the near future. These olefins are industrially employed as building blocks to manufacture a wide range of products, including polymers (polyethylene, polyvinylchloride) and some intermediates of strategic significance. Ethylene is particularly relevant, being one of the most consumed commodities and an indicator of petrochemical development worldwide [1].

Light olefins are currently produced by steam cracking of naphtha or ethane at temperatures above 800 °C, a process with high-energy use, low selectivity, and coking tendency. Therefore, a big research effort is being made to develop more efficient and environmentally friendly technologies. An alternative route for ethylene production is the catalytic oxidative dehydrogenation of ethane (ODHE). This exothermic reaction follows a redox mechanism by which surface lattice oxygen of a metal oxide catalyst is consumed and subsequently restored by gas-phase oxygen. The catalytic oxidative dehydrogenation of ethane does not have the thermodynamic constraints of the non-oxidative process, and the energy balance is favored by the milder operating temperatures [2]. Besides, in an oxidizing atmosphere, coke formation is minimized or directly avoided, and CO_2 emission can be significantly reduced [3].

Powdered catalysts based on nickel oxide are widely reported to be active for ODHE [4–12]. Pure NiO is highly active, but carbon dioxide is preferentially formed [4]. Therefore, selectivity is an important issue to be considered. The addition of a high-valence cation as promoter can enhance ethylene selectivity through the reduction of unselective electrophilic oxygen species [5]. For instance, niobium and tin have been demonstrated to be able to turn the unselective nickel oxide into selective catalysts [5,6]. Other elements such as cerium or zirconium have also shown to be effective promoters for ethylene production [7,8]. Cerium incorporation into the nickel oxide network produces several structural changes, among them the formation of a Ce-Ni solid solution that restrains NiO crystalline growth [7,9]. Moreover, nickel species reducibility and their relative population are modified [10,11].

In contrast with cerium incorporation, which improves ethane conversion both in bulk and supported catalysts [7,9], the addition of zirconium strongly diminishes the activity. Nevertheless, the higher selectivity to ethylene improves the productivity if compared with the unpromoted catalyst [8,12,13]. Due to the Ni-Zr interaction, this promoter modifies the host oxide cell parameters and reducibility [8,12].

Recently, Lee et al. [14] reported enhanced ethylene productivity in Ni-Nb-O/$Ce_xZr_{1-x}O_2$ composite by the promotion of lattice oxygen for Ni-Nb-O; the higher selectivity was attributed to the compensation of lattice oxygen from $Ce_xZr_{1-x}O_2$ into the oxygen vacancy sites.

Another option to enhance selectivity is to disperse the nickel oxide onto a high surface area support, with the advantage of reducing the nickel content compared to bulk formulations. Alumina is an adequate support for this because the changes induced in the nickel oxide electronic structure make it selective to ethylene [4].

At the industrial scale, besides conversion and selectivity, additional parameters come into consideration. For instance, powdered catalysts with sufficiently small particle size to be efficient may not be feasible for real applications. However, this limitation could be overcome if the catalytic formulation is shaped as a structured body.

Cellular structures like foams and channeled monoliths present important advantages over randomly packed fixed bed reactors, such as high geometric surface area per volume and low-pressure drop, among others. In addition, scaling-up can be performed by replication of the structures [15]. However, the manufacture of structured catalysts is not a trivial matter because it usually requires the coating of a substrate, which may strongly influence the final catalytic behavior. For instance, the migration of elements from metallic substrates to the active phase can be negative for the catalyst performance in ODHE, while ceramic materials could enhance catalytic properties [9,16–18]. The first limitation can be overcome in some cases by the formation of a thin layer that acts as a barrier between substrate and catalytic layer. Besides, changing from a powder to a structured form presents numerous challenges such as obtaining good mechanical stability and adherence [19].

In this vein, Zhang et al. [20] developed a microstructured CeO_2-NiO-Al_2O_3/Ni-foam with high mass and heat transfer rates. However, nickel foams are expensive materials to be used in the industry. Alternatively, monolithic reactors have a lower pressure drop due to their high void fraction or open frontal area (0.7–0.9) and their longitudinal channel configuration. Moreover, low-thickness catalyst layers and higher mass transfer coefficients at high gas flows than those of packed beds can be obtained.

In this context, this work reports the development of a novel structured catalyst: Ni-Ce-Zr mixed oxides deposited on a high-surface area extruded alumina monolith. The contribution compares its performance in ODHE with that of the powdered counterpart. This type of monolith was chosen to avoid the migration of different compounds that usually takes place when, for example, stainless steel structures are used. To this end, Ni-Ce-Zr/γ-alumina supported catalysts were prepared first in powder form. The incorporation of both Ce and Zr into the nickel-based formulation as promoters attempts to get a synergistic effect. Then, new γ-alumina monoliths were synthesized as cellular substrates to deposit the Ni-Ce-Zr active phase. All catalysts were exhaustively characterized by X-ray diffraction, Laser Raman spectroscopy, temperature-programmed reduction and X-ray photoelectron spectroscopy, and their catalytic performances were tested in the ODHE reaction. Special emphasis

was put into obtaining high ethylene productivity using a structured catalyst, which constitutes an important issue to be solved for practical applications.

2. Results and Discussion

2.1. Characterization of Active Sites

The synthesized catalysts were identified as $Ni_xCe_yZr_z$-MF, where x, y, and z are the relative atomic fractions of the elements, M is the total metal loading of active phase (wt%), and F indicates the alumina form: powder (P) or homemade monolith (M).

Figure 1 shows the X-ray diffractograms (XRD) of the γ-alumina-supported powder and monolithic catalysts. Those of pure γ-alumina support (powder and monolith) are also included.

The characteristic broad peaks of γ-Al_2O_3 are present in all patterns. Therefore, the crystalline structure of γ-Al_2O_3 is obtained by calcination of extruded boehmite, and it is preserved after the impregnation process. Moreover, the success of the preparation procedure to obtain a structured body with the formulation of the catalytic powder is supported by the similarity of all the diffraction peaks detected, from support and active phase, in the equivalent structured and powdered samples.

The patterns of all the catalysts studied in this work present some peaks that suggest the incipient formation of nickel oxide, NiO (2θ = 37.3°; 43.3°; 62.9°; 75.5° and 79.5°) [18]. At higher Ni loading, the main signal at 43.3° becomes sharper and better defined, showing an increase in the crystalline domain size of this phase, as observed when the total amount of active phase raises from 15 wt% to 25 wt%. At this high Ni loading, the same effect (sharper and better defined NiO peaks) is appreciated at lower Ce/Zr ratios, as a comparison between $Ni_{0.85}Ce_{0.11}Zr_{0.04}$-25P and $Ni_{0.85}Ce_{0.04}Zr_{0.11}$-25P diffractograms points out, which suggests that the incorporation of higher amounts of cerium contributes to NiO dispersion more than zirconium. However, the total active phase loading could have an influence in this tendency, because in the case of $Ni_{0.85}Ce_{0.15}$-15P and $Ni_{0.85}Zr_{0.15}$-15P samples, the crystallinity of the former, with Ce, is higher than that of the Ce-free Zr-containing sample.

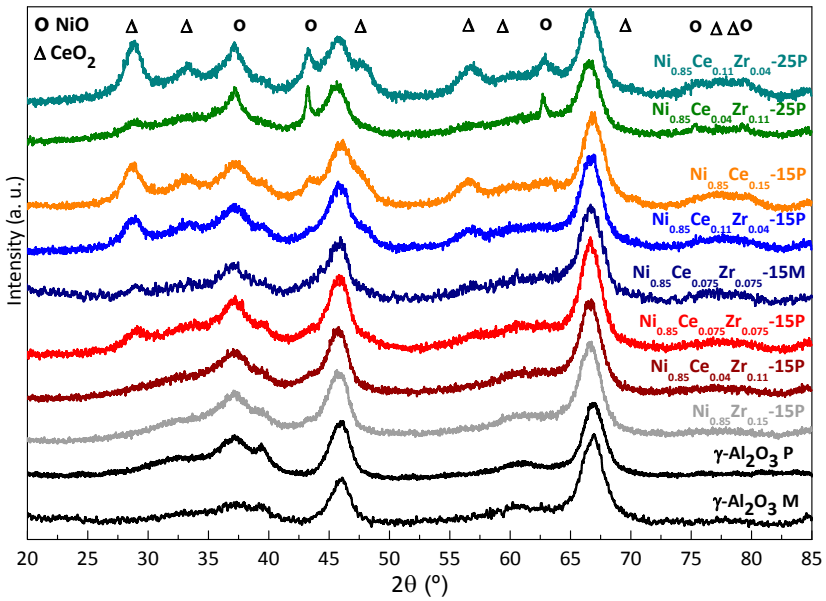

Figure 1. X-ray diffractograms of powder and structured catalysts.

Cerium-containing samples show the diffraction peaks of cerium oxide, CeO_2 (2θ = 28.6°; 33.1°; 47.5°; 56.4°; 59.1°; 69.5°; 76.8° and 79.1°). At higher Ce contents, the peaks are more intense and the full width at half-maximum decreases due to the bigger size of the oxide crystallites. The patterns

of the samples containing 15 wt%, the lower total metal loading, show less defined CeO_2 peaks. The crystallite size of CeO_2 in $Ni_{0.85}Ce_{0.15}$-15P was estimated by the Scherrer´s equation in 3.9 nm, whereas in $Ni_{0.85}Ce_{0.11}Zr_{0.04}$-15P, crystalline CeO_2 is not even detected.

Zirconium oxide (ZrO_2) diffractions corresponding to monoclinic, tetragonal, or cubic crystalline structures were not appreciated in the Zr-containing samples. This suggests low crystallinity or high dispersion of zirconium oxide, or more probably that it was not present as a segregated crystalline phase but forming part of a solid solution.

Since ODHE reaction follows a redox mechanism, the reducibility of the samples was investigated by the temperature-programmed reduction (TPR) technique. The profiles obtained are shown in Figure 2. The broad peak of the samples containing 15 wt% of active phase must be related to at least three kinds of dispersed nickel species with different interaction with the alumina support, designated as α, β and δ, from lower to higher reduction temperatures.

The broad reduction peak of $Ni_{0.85}Ce_{0.15}$-15P sample appears in the 340–850 °C range, with maxima at ca. 420, 595, and 795 °C for the α, β, and δ species, respectively. This zirconium-free catalyst is the most reducible solid of this series. As the zirconium proportion increases, the reduction onset value shifts to higher temperatures, and therefore this promoter somehow hinders the beginning of the reduction. Besides, the maximum of the main peak (β species) shifts from 595 °C, for the Zr-free catalyst, to 640 °C, which corresponds to the Ce-free solid. In contrast, the increasingly higher area of the shoulder located at ~800 °C indicates that δ species, which are less reducible, were preferentially generated at higher Zr content.

Since Ni^{2+} and Zr^{4+} cations have similar ionic radii, it is likely that Zr is introduced into the NiO lattice forming a solid solution, in agreement with the absence of ZrO_2 signals in the XRD patterns. The incorporation of zirconium into the nickel oxide lattice could make Ni^{2+} reduction difficult.

Temperature-Programmed Reduction (TPR) profiles of the 25 wt% catalysts show similar peaks to those of the 15 wt% counterpart, with an additional narrow peak at 340–410 °C, indicative of the presence of bulk crystalline NiO. The formation of the crystalline phase is in complete concordance with X-Ray Diffraction (XRD) results and with the NiO loading that corresponds to the dispersion of a monolayer on alumina, around 12–15 wt% [4]. The low-temperature reduction areas, associated to bulk NiO and α species, were larger in the $Ni_{0.85}Ce_{0.11}Zr_{0.04}$-25P profile than in that of $Ni_{0.85}Ce_{0.04}Zr_{0.11}$-25P, thus confirming the higher reducibility of the former.

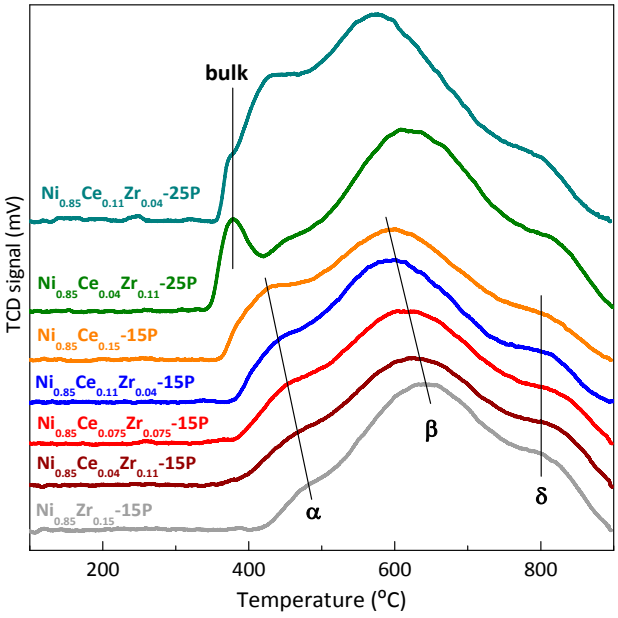

Figure 2. Temperature-programmed reduction profiles of the powder catalysts.

In brief, the samples with higher Ce/Zr ratio are more easily reduced, and this can be related to weaker active phase/support and promoters/Ni interactions, linked to lower Zr amounts, along with a better active phase dispersion related to increasing Ce amount.

Figure 3 shows the laser Raman spectra of the powder and structured catalysts. Remarkably, the spectra, and thus the surface species interplay, are similar in the powder and structured catalysts despite the different synthesis procedures. All samples present a broad, asymmetric band centered at ~550 cm^{-1} assigned to the stretching of Ni-O bond [21,22]. The diminution in the Ce/Zr ratio produces a progressive shift in the Ni-O main band -from 550 cm^{-1} for the zirconium-free catalyst to 560 cm^{-1} for the cerium-free sample-, which has been linked to metal/support interactions and particle size effects [23,24]. However, a similar small shift is detected in the series containing 15 and 25 wt% loading, and thus it is not only a crystallite size effect. This supports the hypothesis of an increasingly strong interplay between the active phase and the support linked to the Ce/Zr ratio, as suggested by the TPR results.

None of the typical Raman bands of tetragonal zirconia (148, 263, 325, 472, 608, and 640 cm^{-1}) or monoclinic zirconia (140, 173, 185, 216, 260, 301, 328, 342, 471, 500, 553, and 632 cm^{-1}) were detected in the spectra of the synthesized catalysts (powder or monolith). This point confirms that crystalline zirconium oxide is not present, not even in the sample with a higher amount of Zr, in agreement with XRD results. Differently, at increasing Ce content in the samples, the characteristic band at 462 cm^{-1} of cerium oxide with fluorite-type structure appears with higher intensity in the spectra, along with two additional bands at 225 and 635 cm^{-1}, directly related to the CeO_2 lattice defects caused by oxygen vacancies and the modification of the oxygen sub-lattice [13,25–31].

It has been reported that the bands at 225 and 635 cm^{-1} point out the formation of a Ni-Ce-O solid solution [13], but in these samples they could also indicate that part of the zirconium is present as a Ce-Zr-O solid solution.

According to the model proposed by Kosacki et al. [26], the size of ceria crystallites can be estimated from Raman spectra, being it inversely proportional to the width at half maximum (FWHM) of its main signal located at ~465 cm^{-1}. The calculated size for the $Ni_{0.85}Ce_{0.15}$-15P catalyst is ~2.6 nm, only slightly smaller than the size calculated by Scherrer's equation from XRD pattern (3.9 nm), which is again evidence of very small crystalline domains. The reason for the difference in the calculated values from both techniques was explained elsewhere [18]. When the amount of incorporated cerium diminishes, the crystallites are even smaller, and therefore the signal broadens, and its intensity quickly decreases, rendering the size calculation impossible.

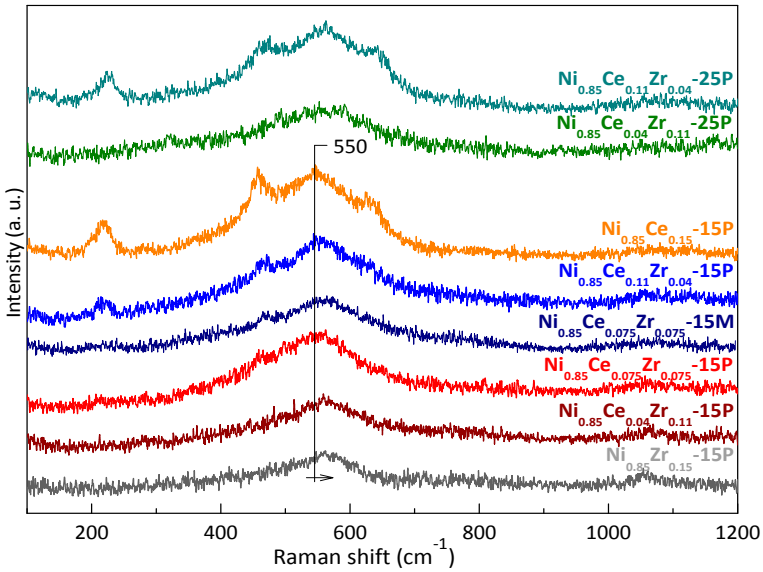

Figure 3. Laser Raman spectra of powder and structured catalysts.

Figure 4 shows the X-ray photoelectron spectra (XPS) of Ni $2p_{3/2}$. The main signal is located at binding energy (BE) values ranging from 856.1 to 856.6 eV, higher than that of the unsupported nickel oxide (854.0 eV) [32], thus demonstrating the presence of Ni^{2+} dispersed on the surface [33,34].

The spin-orbit splitting value, i.e., difference in BE between the main signals of Ni $2p_{3/2}$ and Ni $2p_{1/2}$, is indicative of the state of Ni species. This value is reported to be 18.6 eV for NiO, and lower if the nickel species are present in the surface as aluminate-type, i.e., strongly interacting with the alumina support [4]. The calculated value for each powder catalyst is around 18.0 eV. This strengthens the hypothesis about the strong interaction between Ni species, the support and the promoters that was already inferred from TPR and Raman characterization.

From the XPS results the Ni/Al atomic ratios for the 15 wt% powder catalysts were calculated. They varied from 0.04 to 0.06, showing the highest Ni/Al ratio for the $Ni_{0.85}Ce_{0.11}Zr_{0.04}$-15P formulation. These values are lower than the theoretical ones for this amount of active phase (Ni/Al = 0.13), confirming that a considerable amount of Ni is strongly interacting with the support forming highly dispersed nickel aluminate-type species.

XPS peaks of Zr $3d_{5/2}$ and Zr $3d_{3/2}$ in the zirconium-containing samples appear at 182.0 and 184.2 eV, respectively (not shown). The slightly lower BE values than those reported for ZrO_2 (182.6 and 184.9 eV) [35] are probably related to the interaction of zirconium with the active phase and support by different Zr surroundings. The interplay between cerium and zirconium species is supported by the better resolution obtained in Zr XPS peaks when cerium is present [35]. The signals of Ce $3d_{5/2}$ in the 870–895 eV region could not be properly fitted since they overlapped with those of Ni $2p_{1/2}$.

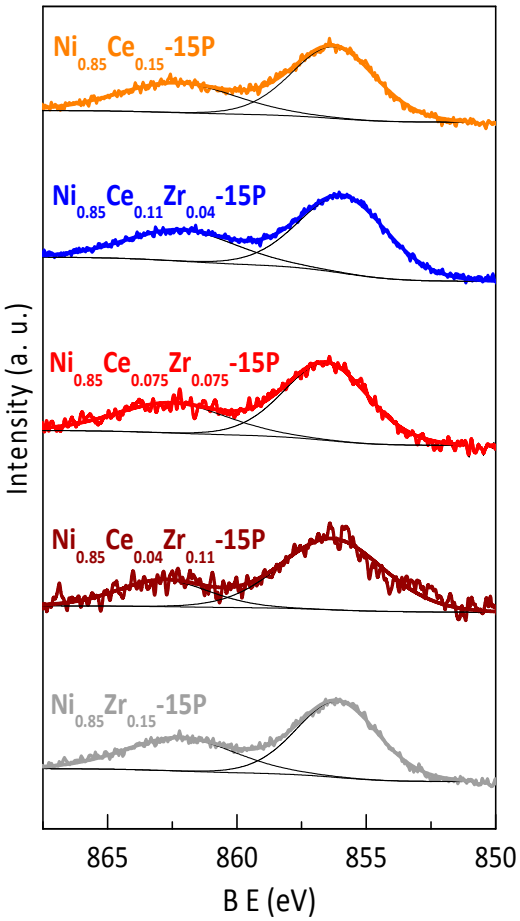

Figure 4. X-ray photoelectron spectroscopy (XPS) spectra of the Ni $2p_{3/2}$ region for the 15 wt% powder catalysts.

2.2. Catalytic Performance in ODHE: Powder and Monolithic Catalysts

First, the influence of the support in the catalytic performance of the samples was evaluated by measuring the activity of pure γ-alumina powder under the same reaction conditions as the samples containing the active phase. At these conditions, the support is practically inert for ODHE, with conversion values lower than 4% at 500 °C and negligible selectivity to ethylene (data not shown). In addition, CO_2 was the main reaction product.

Then, the performance of the powder and the cellular catalyst prepared with the optimal composition was measured: ethane conversion vs. temperature is presented in Figure 5, selectivity to ethylene vs. conversion in Figure 6, the compared evolution of conversion and selectivity with the promoters ratio in Figure 7, and ethylene productivity in Figure 8.

Figure 5 shows ethane conversion as a function of temperature with a catalyst weight to flow rate (W/F) ratio of 0.48 g s cm^{-3}. All catalysts were highly active (30–40% conversion at 450 °C) except for the cerium-free powder, $Ni_{0.85}Zr_{0.15}$-15P, which showed a markedly lower ethane conversion, 11% at 450 °C. This poor activity could be reasonably explained in the light of the characterization results that indicated a strong active phase/support interaction and a hindered reducibility. In addition, the Ni/Al ratio determined by XPS for this sample was the lowest.

Ce is a better activity promoter than Zr because higher Ce/Zr ratios result in higher conversion values. However, there is a synergistic effect when both promoters are present, since the conversion of the sample with the maximum Ce content, i.e. without Zr, significantly drops. Therefore, the highest conversion, an interesting 40% at 450 °C, is obtained with $Ni_{0.85}Ce_{0.11}Zr_{0.04}$ atomic proportion. It is significant to mention that this powder showed the highest Ni/Al ratio on the surface.

By increasing the total metal loading from 15 to 25 wt% the catalyst performance is improved to some extent. Ethane conversion increased from ~31% to ~35% at 450 °C for the lowest Ce/Zr atomic ratio, but the effect was negligible for the other analyzed promoters ratios. Heracleous et al. reported analogous results for unpromoted powdered samples [4].

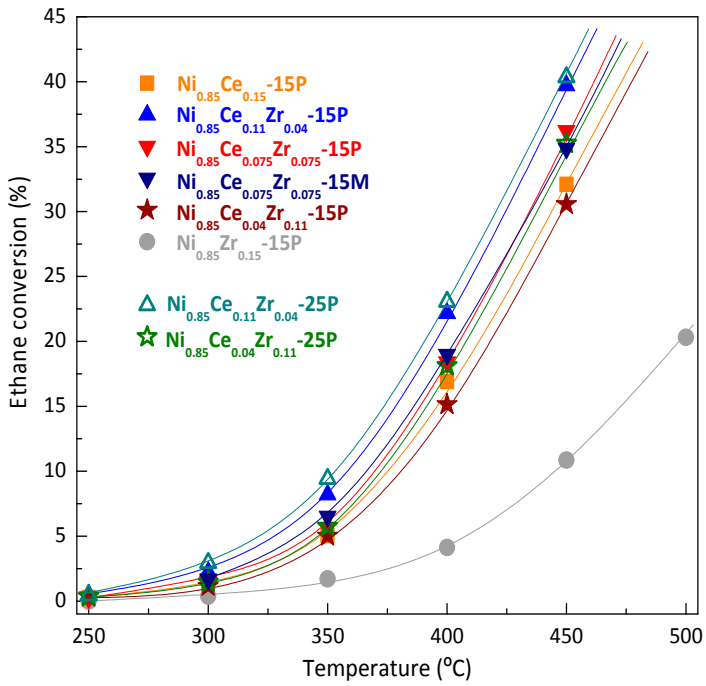

Figure 5. Ethane conversion as a function of temperature of the powder and structured catalysts. Reaction conditions: *T* = variable, W/F (catalyst weight to flow rate) = 0.48 g s cm^{-3}, C_2H_6/O_2 = 1.

The synergistic effect of Ce and Zr promoters in the catalyst is related to the oxygen storage capacity and the transport of oxygen inside the solid structure, fundamental properties for the ODHE reaction, with a redox mechanism [2]. Under reaction conditions, the surface lattice oxygen is consumed and the active sites are reduced to allow the formation of products. Then, the sites are re-oxidized with gas-phase oxygen to restore the initial state. According to the literature, the partial replacement of Ce by Zr produces a Ce-Zr mixed oxide with enhanced properties to transport oxygen [36,37]. The incorporation of elements like Zr^{4+} into the CeO_2 lattice strongly affects the ceria redox properties by increasing its oxygen mobility and storage capacity, even in the presence of nickel or alumina [37–42].

Figure 6 shows the selectivity to ethylene as a function of ethane conversion obtained with different W/F values at 400 °C. The selectivity to ethylene is between 60% and 90% for ethane conversion up to 30%. As a general trend, selectivity decreases at higher conversion, a typical behavior of consecutive catalytic reactions in which the final hydrocarbon product (ethylene) is oxidized.

Samples with higher total loading of active phase (25 wt%) have a slightly less marked decrease, suggesting that ethylene oxidation is favored at lower loadings. For a given active phase composition, the selectivity obtained with 15 wt% samples is higher, an effect that can be related to crystallite sizes of NiO.

Zr is a better selectivity promoter than Ce because the cerium-free solid displayed the highest selectivity values, near 90% at low conversion. In addition, at a given conversion, reduced Ce/Zr ratios favor ethylene formation. This effect is exemplified comparing $Ni_{0.85}Ce_{0.15}$-15P and $Ni_{0.85}Ce_{0.04}Zr_{0.11}$-15P catalysts. The conversion values are similar (Figure 6), but the selectivity is remarkably increased in the sample with Zr (ca. 15% points), raising for instance from 70% to 85% at low conversion (Figure 6). López Nieto et al. had also observed this behavior for two different Ce/Zr ratios in bulk catalysts [43].

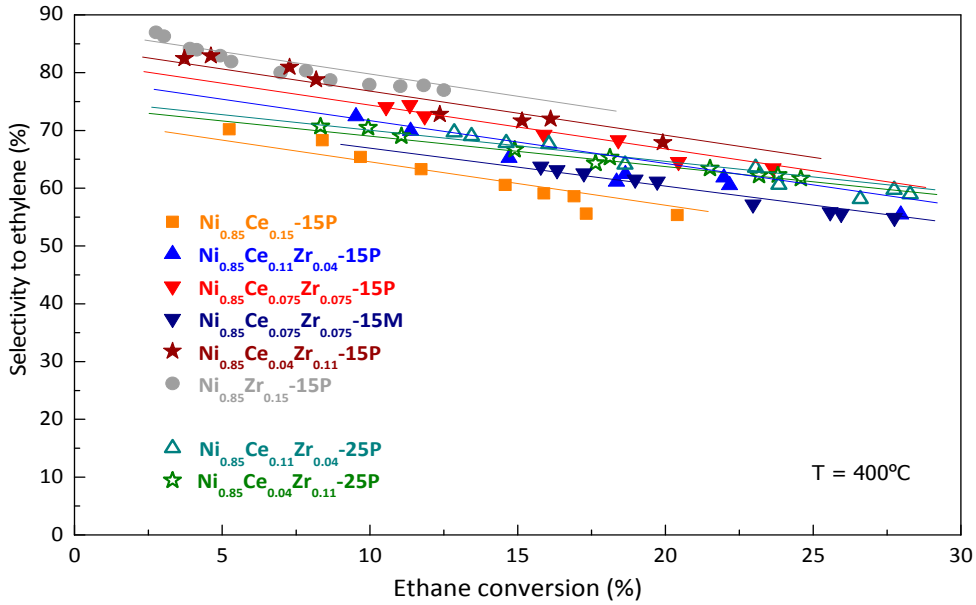

Figure 6. Selectivity to ethylene as a function of ethane conversion of the powder and structured catalysts. Reaction conditions: T = 400 °C, W/F (catalyst weight to flow rate) = variable, C_2H_6/O_2 = 1.

Figure 7 summarizes the effect of the promoters on the catalytic behavior of Ni-based catalysts for the powder samples with 15 wt% metal loading. The graph shows the beneficial effect of Zr promoter on the selectivity to ethylene. The optimal ratio of promoters for Ni-based catalysts on the catalytic performance in ODHE was Ce:Zr = 50:50, at which the product between selectivity and conversion shows a maximum value.

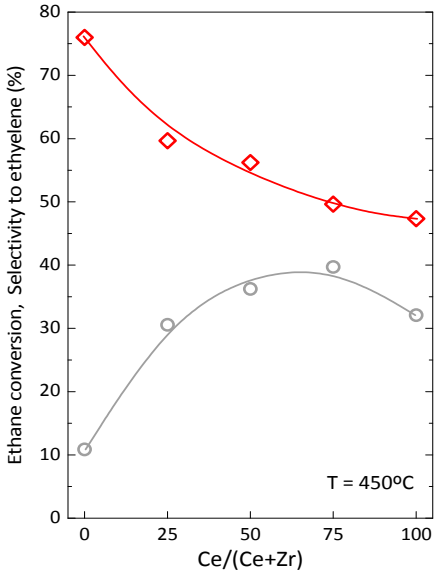

Figure 7. Ethane conversion (○) and ethylene selectivity (◊) at 450 °C as a function of Ce/(Ce+Zr) atomic ratio.

In this vein, ethylene productivity was calculated to assess the global performance of the prepared catalysts. This value takes into account the ethane conversion as well as the selectivity to ethylene. In Figure 8 the productivity of the powdered and monolithic samples with the optimized composition, 6.94 and 6.25 $\mu mol_{ethylene}/g_{act\ cat}$ s, respectively, referred to the weight of active phase, is compared with very recent literature values for ODHE catalysts [14,20,44].

The $Ni_{0.85}Ce_{0.075}Zr_{0.075}$-15P catalyst reached the highest yield. Besides, the performance of the powder sample is only slightly better than that of the monolithic counterpart $Ni_{0.85}Ce_{0.075}Zr_{0.075}$-15 M.

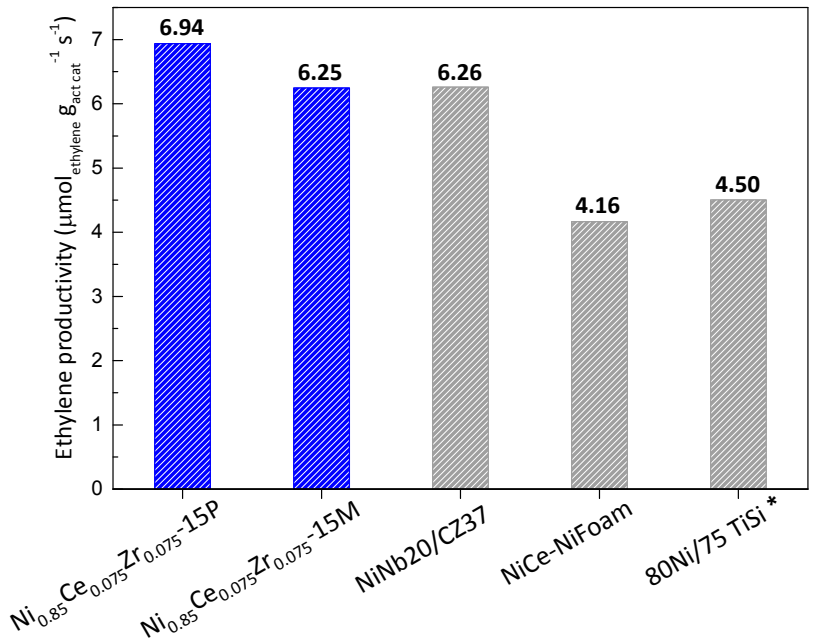

Figure 8. Ethylene productivity at 450 °C (* at 400 °C) for some recent Ni-based catalysts reported in the literature for the oxidative dehydrogenation of ethane. References [14,20,44].

It is worth to mention that the stability of the most efficient catalysts under powder and cellular forms was monitored during 12 h of operation. Ethane conversion and selectivity to ethylene were not significantly modified. Thus, no activity decay was produced due to the satisfactory stability of these analyzed systems.

In the light of the results obtained, the beneficial effect of zirconium on the catalytic performance of the cerium-promoted nickel catalyst could be linked to the formation of a cerium-zirconium solid solution. The presence of Zr has been proven to induce modifications in the active phase/support interplay and the nickel surroundings (TPR, Raman, XPS). The modified active sites are more active and also more selective. The reduction profiles of the zirconium-containing catalysts showed a smaller area of the α species, the ones with a lower interaction with the alumina support. Therefore, the relative amount of these species seems to have a direct effect on the selectivity. A certain amount of zirconium in replacement of cerium not only leads to a significant improvement of the catalytic activity (25%) but also of the selectivity to ethylene.

3. Materials and Methods

The prepared catalysts were designated as $Ni_xCe_yZr_z$-MF, where x, y, and z are the relative atomic fractions, being $x+y+z = 1$. Moreover, M is the total metal loading of active phase (wt%), and F indicates the alumina form: powder (P) or monolith (M).

In all cases, a promoter/nickel atomic ratio (Ce+Zr)/Ni was equal to 0.17, as determined in previous studies for NiCe/γ-Al_2O_3 [9,16].

3.1. Preparation of Powder Catalysts

NiCe, NiZr, and NiCeZr catalysts supported on γ-Al_2O_3 (Puralox® SBA 230, SASOL, Hamburg, Germany) were prepared by wet impregnation with total metal loadings of 15 wt% or 25 wt%. The active phases were incorporated by co-impregnation from solutions of nitrate salts (0.5 M). Then, the samples were dried at 120 °C for 8 h and finally calcined at 500 °C for 2 h.

3.2. Preparation of Cellular Catalysts

Open channel γ-alumina monoliths with a cylindrical shape were prepared by extrusion. Commercial boehmite (Pural® SB1, SASOL, Hamburg, Germany), deionized water and temporary additives were mixed to form a paste with the required rheological properties. Once extruded, the monoliths were dried at room temperature and then calcined at 600 °C for 4 h (Figure 9a).

The active phases were incorporated by impregnation. The monoliths were immersed in the solution of nitrate precursors and then dried overnight at 120 °C. Finally, they were calcined at 500 °C for 2 h (Figure 9b). For comparative reasons, the amount of active phase incorporated (total metal loading per alumina, wt%) was similar in monolith and powder forms. Figure S1 shows that the components were spread homogeneously onto the substrate.

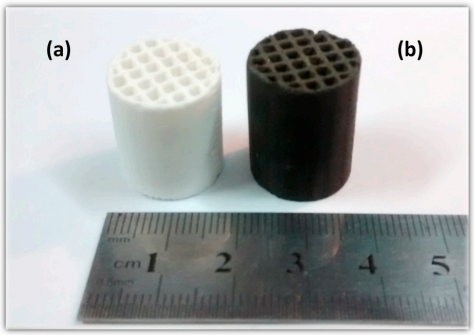

Figure 9. Pictures of alumina monolithic substrate (**a**) and structured catalyst (**b**).

3.3. Catalysts Characterization

Crystalline phases were studied by X-ray diffraction (XRD) with a Phillips PW1710 diffractometer (Phillips, Almelo, Netherlands) operated in 2θ range from 20° to 85° with a scan rate of 1° min^{-1}. Cu-Kα radiation was employed (45 kV voltage and 30 mA current).

Temperature-Programmed Reduction (TPR) experiments were performed employing a Micromeritics Autochem II instrument (Micromeritics, Norcross, GA, USA) with a mixture of 5% H_2/Ar as reducing gas. The heating rate was 10 °C min^{-1} from room temperature to 900 °C.

Laser Raman (LRS) spectra were obtained with a LabRam instrument (Horiba Jobin Yvon, California, CA, USA) coupled to an Olympus confocal microscope, with solid state Laser and CCD-type detector cooled to −70 °C by the Peltier effect (wavelength = 532.13 nm, Laser power = 30 mW, magnification = 100 X). Several sectors of each sample were examined to ensure reproducibility.

X-ray photoelectron spectroscopy (XPS) measurements (SPECS, Berlin, Germany) were performed in a multitechnique equipment with a dual Mg/Al X-ray source and a hemispherical PHOIBOS 150 analyzer operating in the fixed analyzer transmission (FAT) mode. The spectra were obtained with a pass energy of 30 eV and Mg-Kα X-ray source power of 200 W. The pressure in the analyzing chamber was less than 1×10^{-9} mbar. The spectral regions corresponding to Ni 2p, Ce 3d, Zr 3d, O 1s, and C 1s core levels were recorded for each sample. The C 1s signal at 284.6 eV was considered as reference. Peak fitting was performed with the CASAXPS software. The peak areas were determined by integration, employing a Shirley-type background. Peaks were considered as a mixture of Gaussian and Lorentzian functions.

Scanning Electron Microscopy (SEM) and Elemental chemical analysis (EDX, mapping) were performed using a SEM-EDX Phenom ProX instrument (Phenom World, Eindhoven, Netherlands) operated at 15 kV of acceleration voltage. The results were obtained by the theoretical quantitative method (SEMIQ), which does not require standards.

3.4. Catalytic Tests

Catalytic tests were carried out in a flow system operated at atmospheric pressure. The inlet gas composition was 6% oxygen, 6% ethane and helium as balance gas. The analysis of reactants and products was performed with a gas chromatograph Shimadzu GC 2014 (Shimadzu, Kyoto, Japan) equipped with a packed column (HayeSep D) and a thermal conductivity detector (TCD). Carbon monoxide was not detected in any chromatogram obtained from the evaluation of the catalysts. Oxygen never reached complete conversion. Closure of the carbon mass balance was 100 ± 3%.

Two series of experiments were performed. The first one was conducted at variable temperature with a W/F ratio of 0.48 g s cm^{-3} and a total gas flow of 50 cm^3 min^{-1}. In the second set of experiments, different W/F ratios were employed, at a fixed temperature of 400 °C.

The downstream gas composition was measured after 1 h to ensure that the reaction steady state was achieved. The product analysis at each temperature was repeated rigorously three times, with intervals of 30 min.

On the other hand, the reaction experiments were performed three times for the different set of catalysts corresponding to each catalytic formulation. The conversion and selectivity so obtained were almost the same in all cases, considering an experimental error below 5%.

4. Conclusions

A novel $Ni_{0.85}Ce_{0.075}Zr_{0.075}/\gamma$-$Al_2O_3$ cellular catalyst was obtained by the impregnation of an alumina monolith, which was successfully prepared by extrusion and acted simultaneously as substrate and support. The Ni:Ce:Zr molar ratio was adjusted after a careful set of synthesis and catalytic evaluations of powdered catalysts.

NiO and CeO_2 crystalline phases were identified in the powdered samples by XRD depending on the total metal amount and the proportion of promoters.

TPR characterization indicates that the presence of Ce weakens the strong interaction of nickel-zirconium species with the alumina. Furthermore, the incorporation of Zr improves the active phase-support interaction, decreasing in this way the reducibility of Ni.

A fraction of Ni forms a solid solution with Ce (Ni-Ce-O) according to Raman spectroscopy results. This phase may also contain zirconium ions, since their presence was detected by XPS, but segregated zirconium oxide was not identified with the characterization techniques employed.

All formulations were highly active and selective in the oxidative dehydrogenation of ethane with a maximum ethylene productivity of 6.94 $\mu mol_{ethylene}\ g_{act\ cat}{}^{-1}\ s^{-1}$. In this respect, the addition of cerium increases the population of the most reducible nickel species, which would benefit ethane conversion. Meanwhile, the incorporation of zirconium would boost ethylene selectivity through the generation of higher amounts of the least reducible nickel species. Therefore, the partial replacement of cerium by zirconium changes the characteristics of the active sites, thus increasing the global efficiency of the Ni-based catalysts. Besides, it is likely that the formation of Ni-Ce-(Zr)-O phase generates catalysts with optimized properties. A clear synergistic effect between Ce and Zr was verified.

The most efficient powder formulation, $Ni_{0.85}Ce_{0.075}Zr_{0.075}$-15P, was effectively reproduced under a novel structured form through the development of an alumina monolithic substrate. The active phase/support interactions and the main features of the active sites were successfully preserved in the structured system, which showed similar ethylene production to that of the powdered form. Besides the advantages of being a structured catalyst, the novel system presented here shows productivity values among the best reported so far (by active phase amount), which makes it a promising catalyst for practical applications.

Supplementary Materials: The following are available online at www.mdpi.com/2073-4344/7/11/331/s1, Figure S1: SEM micrographs of the cellular catalyst and distribution of the elements (mapping).

Acknowledgments: The authors wish to acknowledge the financial support received from ANPCyT, CONICET, UNL, and Spanish CTQ-2014-57578-R and CAM S2013/MAE-2985 projects. Thanks are given to ANPCyT for the acquisition of the SPECS multitechnique analysis instrument (PME 8-2003) and to the Grant PME 87-PAE 36985 for the purchase of the Raman Instrument. Special thanks are also given to E. D. Banús for his help with Raman experiments and to Dra. M. A. Ulla for the fruitful discussions.

Author Contributions: Juan Pablo Bortolozzi performed some characterization experiments and catalytic tests. Raquel Portela carried out the synthesis of the monolithic catalysts and she contributed to the characterization of the samples. Viviana Milt, Pedro Ávila, and Eduardo Miró organized the manuscript distribution and supervised the work advising about the discussion and the conclusion sections. Finally, Juan Pablo Bortolozzi wrote the article under direction and agreement of the other authors.

Conflicts of Interest: The authors declare no conflict of interest.

References

1. Chu, B.; Truter, L.; Nijhuis, T.A.; Cheng, Y. Oxidative dehydrogenation of ethane to ethylene over phase-pure M1 $MoVNbTeO_x$ catalysts in a micro-channel reactor. *Catal. Sci. Technol.* **2015**, *5*, 2807–2813. [CrossRef]
2. Gärtner, C.A.; van Veen, A.C.; Lercher, J.A. Oxidative dehydrogenation of ethane: Common principles and mechanistic aspects. *ChemCatChem* **2013**, *5*, 3196–3217. [CrossRef]
3. Védrine, J.C. Heterogeneous partial (amm)oxidation and oxidative dehydrogenation catalysis on mixed metal oxides. *Catalysts* **2016**, *6*, 22–48. [CrossRef]
4. Heracleous, E.; Lee, A.F.; Wilson, K.; Lemonidou, A.A. Investigation of Ni-based alumina-supported catalysts for the oxidative dehydrogenation of ethane to ethylene: Structural characterization and reactivity studies. *J. Catal.* **2005**, *231*, 159–171. [CrossRef]
5. Heracleous, E.; Lemonidou, A.A. Ni-Me-O mixed metal oxides for the effective oxidative dehydrogenation of ethane to ethylene - Effect of promoting metal Me. *J. Catal.* **2010**, *270*, 67–75. [CrossRef]
6. Solsona, B.; López Nieto, J.M.; Agouram, S.; Soriano, M.D.; Dejoz, A.; Vázquez, M.I.; Concepción, P. Optimizing both catalyst preparation and catalytic behaviour for the oxidative dehydrogenation of ethane of Ni-Sn-O catalysts. *Top. Catal.* **2016**, *59*, 1564–1572. [CrossRef]

7. Solsona, B.; Concepción, P.; Hernández, S.; Demicol, B.; López Nieto, J.M. Oxidative dehydrogenation of ethane over NiO-CeO_2 mixed oxides catalysts. *Catal. Today* **2012**, *180*, 51–58. [CrossRef]
8. Wu, Y.; Gao, J.; He, Y.; Wu, T. Preparation and characterization of Ni-Zr-O nanoparticles and its catalytic behavior for ethane oxidative dehydrogenation. *Appl. Surf. Sci.* **2012**, *258*, 4922–4928. [CrossRef]
9. Bortolozzi, J.P.; Gutierrez, L.B.; Ulla, M.A. Efficient structured catalysts for ethylene production through the ODE reaction: Ni and Ni-Ce on ceramic foams. *Catal. Commun.* **2014**, *43*, 197–201. [CrossRef]
10. Smoláková, L.; Kout, M.; Koudelková, E.; Čapek, L. The role of Ni species distribution on the effect of Ce as a promoter in C_2-ODH reaction. *Top. Catal.* **2015**, *58*, 843–853. [CrossRef]
11. Smoláková, L.; Kout, M.; Koudelková, E.; Čapek, L. Effect of calcination temperature on the structure and catalytic performance of the Ni/Al_2O_3 and Ni-Ce/Al_2O_3 catalysts in oxidative dehydrogenation of ethane. *Ind. Eng. Chem. Res.* **2015**, *54*, 12730–12740. [CrossRef]
12. Bortolozzi, J.P.; Banús, E.D.; Courtalón, N.L.; Ulla, M.A.; Milt, V.G.; Miró, E.E. Flexible NiZr-based structured catalysts for ethylene production through ODH of ethane: Catalytic performance enhancement. *Catal. Today* **2016**, *273*, 252–258. [CrossRef]
13. Bortolozzi, J.P.; Banús, E.D.; Milt, V.G.; Miró, E.E. New formulations of Ni-containing ceramic papers to enhance the catalytic performance for the oxidative dehydrogenation of ethane. *Ind. Eng. Chem. Res.* **2014**, *53*, 17570–17579. [CrossRef]
14. Lee, M.; Yun, Y.S.; Sung, J.; Lee, J.; Seo, Y.-J.; Song, I.K.; Yi, J. Enhanced ethylene productivity by the promotion of lattice oxygen in Ni-Nb-O/$Ce_xZr_{1-x}O_2$ composite for oxidative dehydrogenation of ethane. *Catal. Commun.* **2017**, *95*, 58–62. [CrossRef]
15. Kreutzer, M.T.; Kapteijn, F.; Moulijn, J.A. Shouldn't catalysts shape up? Structured reactors in general and gas-liquid monolith reactors in particular. *Catal. Today* **2006**, *111*, 111–118. [CrossRef]
16. Bortolozzi, J.P.; Banús, E.D.; Terzaghi, D.; Gutierrez, L.B.; Milt, V.G.; Ulla, M.A. Novel catalytic ceramic papers applied to oxidative dehydrogenation of ethane. *Catal. Today* **2013**, *216*, 24–29. [CrossRef]
17. Brussino, P.; Bortolozzi, J.P.; Milt, V.G.; Banús, E.D.; Ulla, M.A. NiCe/γ-Al_2O_3 coated onto cordierite monoliths applied to oxidative dehydrogenation of ethane (ODE). *Catal. Today* **2016**, *273*, 259–265. [CrossRef]
18. Bortolozzi, J.P.; Weiss, T.; Gutierrez, L.B.; Ulla, M.A. Comparison of Ni and Ni-Ce/Al_2O_3 catalysts in granulated and structured forms: Their possible use in the oxidative dehydrogenation of ethane reaction. *Chem. Eng. J.* **2014**, *246*, 343–352. [CrossRef]
19. Rasmussen, S.B.; López-Medina, R.; Portela, R.; Mikolajska, E.; Daturi, M.; Ávila, P.; Bañares, M.A. Shaping up operando spectroscopy: Raman characterization of a working honeycomb monolith. *Catal. Sci. Technol.* **2015**, *5*, 4942–4945. [CrossRef]
20. Zhang, Z.; Han, L.; Chai, R.; Zhang, Q.; Li, Y.; Zhao, G.; Liu, Y.; Lu, Y. Microstructured CeO_2-NiO-Al_2O_3/Ni-foam catalyst for oxidative dehydrogenation of ethane to ethylene. *Catal. Commun.* **2017**, *88*, 90–93. [CrossRef]
21. Ni, X.; Zhao, Q.; Zhou, F.; Zheng, H.; Cheng, J.; Li, B. Synthesis and characterization of NiO strips from a single source. *J. Cryst. Growth* **2006**, *289*, 299–302. [CrossRef]
22. Savova, B.; Loridant, S.; Filkova, D.; Millet, J.M.M. Ni-Nb-O catalysts for ethane oxidative dehydrogenation. *Appl. Catal. A Gen.* **2010**, *390*, 148–157. [CrossRef]
23. Yadav, S.K.; Jeevanandam, P. Synthesis of NiO-Al_2O_3 nanocomposites by sol-gel process and their use as catalyst for the oxidation of styrene. *J. Alloys Compd.* **2014**, *610*, 567–574. [CrossRef]
24. Duan, W.J.; Lu, S.H.; Wu, Z.L.; Wang, Y.S. Size effects on properties of NiO nanoparticles grown in alkali salts. *J. Phys. Chem. C* **2012**, *116*, 26043–26051. [CrossRef]
25. Liu, X.; Zuo, Y.; Li, L.; Huang, X.; Li, G. Heterosturcture NiO/$Ce_{1-x}Ni_xO_2$: Synthesis and synergistic effect of simultaneous surface modification and internal doping for superior catalytic performance. *RSC Adv.* **2014**, *4*, 6397–6406. [CrossRef]
26. Kosacki, I.; Suzuki, T.; Anderson, H.U.; Colomban, P. Raman scattering and lattice defects in nanocrystalline CeO_2 thin films. *Solid State Ion.* **2002**, *149*, 99–105. [CrossRef]
27. Kim, B.K.; Hamaguchi, H. Mode assignments of the Raman spectrum of monoclinic zirconia by isotopic exchange technique. *Phys. Status Solidi* **1997**, *203*, 557–563. [CrossRef]
28. Yamamoto, T.; Tanaka, T.; Takenaka, S.; Yoshida, S.; Onari, T.; Takahashi, Y.; Kosaka, T.; Hasegawa, S.; Kudo, M. Structural analysis of iron and manganese species in iron- and manganese-promoted sulphated zirconia. *J. Phys. Chem. B* **1999**, *103*, 2385–2393. [CrossRef]

29. Ali, T.T.; Narasimharao, K.; Ahmed, N.S.; Basahel, S.; Al-Thabaiti, S.; Mokhtar, M. Nanosized iron and nickel oxide zirconia supported catalysts forbenzylation of benzene: Role of metal oxide support interaction. *Appl. Catal. A Gen.* **2014**, *486*, 19–31. [CrossRef]
30. Hoang, T.M.C.; Rao, N.K.; Lefferts, L.; Seshan, K. Investigation of Ce-Zr oxide-supported Ni catalysts in the steam reforming of meta-cresol as a model component for bio-derived tar. *ChemCatChem* **2015**, *7*, 468–478. [CrossRef]
31. Zhang, F.; Chen, C.-H.; Hanson, J.C.; Robinson, R.D.; Herman, I.P.; Chan, S.-W. Phases in ceria-zirconia binary oxide $(1-x)CeO_{2-x}ZrO_2$ nanoparticles: The effect of particle size. *J. Am. Ceram. Soc.* **2006**, *89*, 1028–1036. [CrossRef]
32. AbdelDayem, H.M.; Faiz, M.; Abdel-Samad, H.S.; Hassan, S.A. Rare earth oxides doped NiO/γ-Al_2O_3 catalyst for oxidative dehydrogenation of cyclohexane. *J. Rare Earths* **2015**, *33*, 611–618. [CrossRef]
33. Ding, C.; Gao, W.; Zhao, Y.; Zhao, Y.; Zhou, H.; Li, J.; Jin, H. Effects of Co^{2+} doping on physicochemical behavior of hierarchical NiO nanostructure. *Appl. Surf. Sci.* **2016**, *390*, 890–896. [CrossRef]
34. Jiménez-González, C.; Boukha, Z.; Rivas, B.; Delgado, J.J.; Cauqui, M.A.; González-Velasco, J.R.; Gutiérrez-Ortiz, J.I.; López-Fonseca, R. Structural characterization of Ni/alumina reforming catalysts activated at high temperatures. *Appl. Catal. A Gen.* **2013**, *466*, 9–20. [CrossRef]
35. Kaminski, P.; Ziolek, M. Surface and catalytic properties of Ce-, Zr-, Au-, Cu-modified SBA-15. *J. Catal.* **2014**, *312*, 249–262. [CrossRef]
36. Duprez, D. Study of surface reaction mechanisms by $^{16}O/^{18}O$ and H/D isotopic exchange. *Catal. Today* **2006**, *112*, 17–22. [CrossRef]
37. Murota, T.; Hasegawa, T.; Aozasa, S.; Matsui, H.; Motoyama, M. Production method of cerium oxide with high storage capacity of oxygen and its mechanism. *J. Alloys Compd.* **1993**, *193*, 298–299. [CrossRef]
38. Srinivas, D.; Satyanarayana, C.V.V.; Potdar, H.S.; Ratnasamy, P. Structural studies on NiO-CeO_2-ZrO_2 catalysts for steam reforming of ethanol. *Appl. Catal. A Gen.* **2003**, *246*, 323–334. [CrossRef]
39. Pastor-Pérez, L.; Ramírez Reina, T.; Ivanova, S.; Centeno, M.A.; Odriozola, J.A.; Sepúlveda-Escribano, A. Ni-CeO_2/C catalysts with enhanced OSC for the WGS reaction. *Catalysts* **2015**, *5*, 298–309. [CrossRef]
40. Wang, J.; Wen, J.; Shen, M. Effect of interaction between $Ce_{0.7}Zr_{0.3}O_2$ and Al_2O_3 on structural characteristics, thermal stability, and oxygen storage capacity. *J. Phys. Chem. C* **2008**, *112*, 5113–5122. [CrossRef]
41. Azambre, B.; Zenboury, L.; Weber, J.V.; Burg, P. Surface characterization of acidic ceria-zirconia prepared by direct sulfation. *Appl. Surf. Sci.* **2010**, *256*, 4570–4581. [CrossRef]
42. Si, Z.; Weng, D.; Wu, X.; Ma, Z.; Ma, J.; Ran, R. Lattice oxygen mobility and acidity improvements of NiO-CeO_2-ZrO_2 catalyst by sulfation for NO_x reduction by ammonia. *Catal. Today* **2013**, *201*, 122–130. [CrossRef]
43. López Nieto, J.M.; Solsona, B.; Grasselli, R.K.; Concepción, P. Promoted NiO catalysts for the oxidative dehydrogenation of ethane. *Top. Catal.* **2014**, *57*, 1248–1255. [CrossRef]
44. Ykrelef, A.; Nadji, L.; Issaadi, R.; Agouram, S.; Rodríguez-Castellón, E.; Solsona, B.; López Nieto, J.M. Mixed oxide Ti-Si-O prepared by non-hydrolytic xerogel method as a diluter of nickel oxide for the oxidative dehydrogenation of ethane. *Catal. Today* **2017**. [CrossRef]